

Article

Not peer-reviewed version

---

# Combined Transcriptomic and Proteomic Profiling Uncovers Developmental Dynamics of Autophagy in the Cortex

---

[Francesca Nuzzolillo](#)<sup>†</sup>, [Clarissa Braccia](#)<sup>†</sup>, [Annapaola Andolfo](#), Stefano de Pretis, [Michela Palmieri](#)<sup>\*</sup>

Posted Date: 26 February 2026

doi: 10.20944/preprints202602.1768.v1

Keywords: autophagy; lysosome; cortical development; synapsis; transcriptomic; proteomic



Preprints.org is a free multidisciplinary platform providing preprint service that is dedicated to making early versions of research outputs permanently available and citable. Preprints posted at Preprints.org appear in Web of Science, Crossref, Google Scholar, Scilit, Europe PMC.

Copyright: This open access article is published under a [Creative Commons CC BY 4.0 license](#), which permit the free download, distribution, and reuse, provided that the author and preprint are cited in any reuse.

Disclaimer/Publisher's Note: The statements, opinions, and data contained in all publications are solely those of the individual author(s) and contributor(s) and not of MDPI and/or the editor(s). MDPI and/or the editor(s) disclaim responsibility for any injury to people or property resulting from any ideas, methods, instructions, or products referred to in the content.

Article

# Combined Transcriptomic and Proteomic Profiling Uncovers Developmental Dynamics of Autophagy in the Cortex

Francesca Nuzzolillo <sup>1,†</sup>, Clarissa Braccia <sup>2,†</sup>, Annapaola Andolfo <sup>2</sup>, Stefano de Pretis <sup>3</sup> and Michela Palmieri <sup>1,4,\*</sup>

<sup>1</sup> Vita-Salute San Raffaele University, Milan, Italy

<sup>2</sup> ProMeFa, Proteomics and Metabolomics Facility, IRCCS San Raffaele Scientific Institute, Milan, Italy

<sup>3</sup> Center for Omics Sciences, IRCCS San Raffaele Scientific Institute, Milan, Italy

<sup>4</sup> Rett syndrome and neurodevelopmental disorders, Division of Neuroscience, IRCCS San Raffaele Scientific Institute, Milan, Italy

\* Correspondence: palmieri.michela@hsr.it

† These authors contributed equally.

## Abstract

Autophagy is an evolutionarily conserved degradation and recycling process through which cells deliver cytoplasmic components such as toxic or defective proteins and organelles to lysosomes for clearance. Unlike dividing cells, neurons depend on degradative pathways to prevent the buildup of cellular waste and to sustain nutrient and energy homeostasis. Emerging evidence indicates that autophagy is particularly critical during early development when neuronal circuits are being established, synaptic connections refined, and activity-dependent mechanisms sculpt overall network architecture. Accordingly, loss of key autophagy-related genes in newly formed neurons disrupts differentiation, synaptic formation and neurotransmission. Despite these insights, the developmental regulation of autophagy genes remains poorly understood, and the composition of the autophagic machinery at synapses is still largely unresolved. To address this, we performed genome-wide transcriptomic analyses of the cortical brain region to characterize the maturation-dependent dynamics of autophagy-lysosomal genes. In parallel, we examined the autophagy-associated proteome within synaptosomes to better understand how autophagic proteins contribute to synaptic processes during critical stages of network formation. Together, these complementary approaches reveal new aspects of autophagy regulation during development and provide a foundation for identifying therapeutic targets for neurological disorders linked to impaired synaptic and cellular homeostasis.

**Keywords:** autophagy; lysosome; cortical development; synapsis; transcriptomic; proteomic

## 1. Introduction

Macroautophagy (hereafter referred to as autophagy) is an evolutionary conserved process devoted to the elimination of detrimental cellular components like dysfunctional organelles, toxic macromolecules and unfolded proteins [1]. It is particularly important in neurons, which are post-mitotic cell, metabolically very active and highly vulnerable to any loss of cellular homeostasis [2]. Consistent with this, defective autophagy function has been linked to aging and neurodegenerative diseases [3–5]. Interestingly, increasing evidence also indicates that autophagy is involved in multiple stages of neurodevelopment including neuronal differentiation, neurite overgrowth, neurite guidance, as well as formation and refinement of synaptic connections. For instance, loss of the autophagy-related gene 5 (Atg5) in dividing neural progenitor cells (NPCs) within the adult

hippocampus led to reduced autophagic flux and delayed neuronal maturation [6]. Similarly, deletion of ATG7 in hypothalamic proopiomelanocortin (POMC) neurons caused loss of axonal projections, highlighting the essential role of autophagy in supporting axonal growth in vivo [7]. Moreover, disruption of core autophagy genes in rodent neurons has been shown to alter multiple aspects of synaptic function including synaptic maturation, assembly, neurotransmitter release, and neuronal plasticity [8–10]. Furthermore, autophagy may regulate synapses by directly degrading key synaptic protein substrates. Post-synaptic scaffolds PSD-95, PICK1 and SHANK3, which are crucial for dendritic spine remodeling, were identified as autophagic cargos [8]. Finally, mutations in genes encoding for regulators and components of the autophagic-lysosomal system have been linked to neurodevelopmental disorders and childhood-onset neurological diseases [11–14]. All these findings suggest that autophagy regulates at different level neuronal maturation and synaptic machinery, however, how it modulates all these processes is still missing.

Recent omics-based studies, particularly RNA sequencing coupled with pathway enrichment analyses, have been extensively used to investigate autophagy, largely in the context of pathological conditions, highlighting the strong association between autophagy dysregulation and disease onset or progression. Alongside these advances, the identification of the transcription factors TFEB and TFE3, members of the basic helix–loop–helix leucine zipper family, has revealed the existence of a transcriptional program that coordinates the expression of autophagy and lysosomal genes [15–17]. Despite these important discoveries, most transcriptomic and bioinformatic analyses have focused on disease-related or stress-induced autophagy. Consequently, the regulation of autophagy under basal physiological conditions—particularly during brain development—remains largely unexplored. To investigate this, we performed a comprehensive transcriptomic analysis of the cortical brain region to define the core set of autophagy-lysosomal gene expressed throughout distinct stages of brain maturation, including neurogenesis, axon and dendritic growth, and synaptogenesis. To elucidate how autophagy contributes to synaptic function, we also characterized the proteomic landscape of synaptosomes, focusing on the autophagy-associated proteins that operate at developing synapses. These findings advance our understanding of how neuronal autophagy is developmentally regulated and whether it contributes to the establishment and maintenance of synaptic connectivity. Moreover, this work provides novel insight into mechanisms that may explain synaptic vulnerability in neurodevelopmental disorders and highlights potential therapeutic targets for these conditions.

## 2. Materials and Methods

### *Animals*

Wild-type (WT) male and female mice (*Mus musculus*) were obtained from Charles River Laboratories and housed in an SPF facility (IRCCS San Raffaele Scientific Institute, Milan), with 12h light/dark cycle, food and water ad libitum. All experiments involving animals were performed upon authorization from the Italian Ministry of Health, according to international guidelines for animal welfare (European Directive 2010/63/EU).

### *Total RNA extraction*

Total RNA was extracted from the cerebral cortices of wild-type (WT) mice at embryonic day 16 (E16), postnatal day 5 (P5), and postnatal day 10 (P10) using the Qiagen RNeasy Mini Kit (50), following the manufacturer's instructions. Immediately after dissection, tissues were snap-frozen on dry ice and stored at  $-80^{\circ}\text{C}$  until RNA extraction. On-column DNase I digestion was performed to eliminate residual genomic DNA. RNA concentration and purity were measured using a NanoDrop spectrophotometer (Thermo Fisher Scientific), and RNA integrity was assessed using an Agilent 2100 Bioanalyzer. Only samples with an RNA Integrity Number (RIN)  $\geq 8$  were used for downstream analyses.

### *Real-time qPCR*

Total RNA from six male and six females per each time point (E16, P5 and P10) were extracted and reverse transcribed using the QuantiTect Reverse Transcription Kit (Qiagen), starting from 1  $\mu\text{g}$

of total RNA. Gene expression was analyzed by real-time PCR (qPCR) using a SYBR Green-based Master Mix. Reactions were performed in technical triplicates under standard amplification conditions, followed by a melting curve analysis to assess product specificity. Relative gene expression was calculated using the  $\Delta\Delta C_t$  method, with cyclophilin as the housekeeping gene. Data analysis was carried out using GraphPad Prism and differences were considered statistically significant at  $p < 0.05$ . Primers used for the expression gene analysis were the following:

Gene name	Primer forward 5'-3'	Primer reverse 5'-3'
<i>Atg9a</i>	GCGTTGCTGGTCACTCTATG	CAGGATAGAGCCAGCGAAGA
<i>Atg16l1</i>	TCGCCTCAATGCAGAGAATG	GAGGTTCCCTTTGCTGCTTCT
<i>Atp6v0c</i>	CAGAGCTGATCATGAAGTCCATC	GAAAACTCCTGTAGATGATG
<i>Atp6v1d</i>	GGATTGAACGCACCCTTG	GCTGCTCTCCGCCGCTC
<i>Bdnf</i>	AAGTCTGCATTACATTCTCGA	GTTTTCTGAAAGAGCGACAGTT
<i>C-fos</i>	AGAGCGCCCCATCCTTAC	GCAGCCATCTTATTCCGTTT
<i>Cln3</i>	CCTGGCTGCTGATGTTATGA	TGAGGGCAAATCCACTAAT
<i>Ctsa</i>	TTCTGATCCAGCCAGATGGTG	TACAGCACGTTGGCAATCAGG
<i>Ctsd</i>	CGTCCTTTGACATCCACTACGG	TGGAACCGATACAGTGTCTG
<i>Cyclophilin</i>	GGCAAATGCTGGACCAAACACAA	GTAAAATGCCCGCAAGTCAAAG
<i>Egr1</i>	CCTTCAATCCTCAAGGGAGC	AACCGAGTCGTTTGGCTGGGA
<i>Foxo1</i>	GTGGATGGTGAAGAGCGTGCCC	GCTGTGAAGGGACAGATTGTGGCG
<i>Foxo3</i>	AAGGGCGACAGCAACAGCTCTG	CATGAAGCGGCTGTGCAGGGAC
<i>Gabarapl1</i>	CAAAGAGGAGCATCCGTTTCGAG	TTGTCCAGGTCTCCTATCCGAG
<i>Glb1</i>	AAATGGCTGGCAGTCTTCTG	ACCTGCACGGTTATGATCGGT
<i>Hexa</i>	CTACATCCAGACGCTGCTGGAC	TACTGGCATTCTTCCCGCCAC
<i>Hif1-<math>\alpha</math></i>	GCTGAAGACACAGAGGCAAA	TACTTGGAGGGCTTGGAGAA
<i>Lamp1</i>	CCTACGAGACTGCGAATGGT	CCACAAGAACTGCCATTTTTTC
<i>Map1lc3b</i>	GCTTGCAGCTCAATGCTAAC	CCTGCGAGGCATAAACCATGTA
<i>Mcol1</i>	GCGCCTATGACACCATCAA	TATCCTGGCACTGCTCGAT
<i>Naglu</i>	TCCAACAGCACGAGTTTGAG	CTGCGATGGCTAATCTGTCA
<i>Pgc1-<math>\alpha</math></i>	GAATCAAGCCACTACAGACACGC	CATCCCTCTTGAGCCTTTCGTG
<i>Slc38a9</i>	TTGAAAGCGAGGGAAATGATGGTC	ATGGGAATGAGGGTCACTGAGAAG
<i>Sqstm1</i>	GAAGCTGCCCTATACCCACA	TGGGAGAGGGACTCAATCAG
<i>Tfe3</i>	AGGATCAAAGAGCTGGGCAC	CCGGCTCTCCAGGTCTTTG
<i>Tfeb</i>	GTCATTGACAACATTATGCGCC	GCGTGTTAGGCATCTTGCATCT
<i>Thpp1</i>	CCCCTCATGTGGATTTTGTGG	TGGTTCTGGACGTTGTCTTGG
<i>Ulk1</i>	TGGAGACCTGGCTGACTACCTGC	TGGATGATGCCCTTGCTGTGCA

### RNAseq and data processing

Total RNA was extracted from five to eight males and females WT cortices pooled together. Only high-quality RNA with an RNA Integrity Number (RIN) of 9 or higher was used. Library preparation and sequencing have been performed with TruSeq RNA Library Preparation Kit v2 (Illumina) by Genewiz. FASTQ sequencing reads were adaptor-trimmed and quality-filtered with Trimmomatic [30], prior to mapping to the mm10 mouse reference genome (<https://www.gencodegenes.org/mouse/>) with STAR [31]. Gene counts were obtained using featureCounts [32]. Normalization and differential gene expression analysis (DEG) have been performed with DESeq2 [33]. Only genes with sufficient expression levels were included in the DGE

testing. Specifically, 9,211 genes exhibiting an average expression of at least 5 FPKM and a minimum of 10 counts in at least one of the three profiled conditions (E16, P5, or P10) were considered for analysis. Heatmap visualization and clustering were performed using the R package pheatmap. Gene ontology enrichment analysis and GSEA were performed using the R package clusterProfiler [34].

#### ***Synaptosome Enrichment Procedure***

Synaptosomes were isolated from the cerebral cortices of wild-type mice at postnatal days P5, P10, and P20, with three to four biological replicates per time point. For each replicate, half of the cortex from a male mouse and half from a female mouse were pooled. The extraction buffer was prepared using 0.32 M sucrose and 4 mM HEPES, supplemented with protease and phosphatase inhibitors to preserve protein integrity. Cortical tissue was mechanically homogenized on ice using a Potter-Elvehjem homogenizer. The homogenate was subjected to differential centrifugation as follows: 800 × g for 3 minutes at 4°C to remove nuclei and debris, followed by 800 × g for 15 minutes at 4°C, and finally 10,200 × g for 15 minutes at 4°C. The resulting pellet, containing the synaptosomal fraction, was carefully collected and resuspended in lysis buffer containing 1% SDS for downstream western blot and proteomic analysis. Protein concentration of the synaptosomal lysates was quantified using the bicinchoninic acid (BCA) assay (Pierce™ BCA Protein Assay Kit), following the manufacturer's instructions. Equal amounts of protein (30 µg) were then processed for label-free quantitative proteomics.

#### ***Western blotting***

Protein lysates were separated by SDS-PAGE. Briefly, 10 µg of protein per sample were loaded onto 10% or 12% TGX gels and run in running buffer (25 mM Tris, 192 mM glycine, 0.1% SDS) at 100 V. Proteins were transferred onto nitrocellulose membranes using a semidry transfer system (Trans-blot Turbo Transfer system, Bio-Rad) according to the manufacturer's instructions. Blocking and incubation with primary and HRP-conjugated secondary antibodies (Jackson ImmunoResearch) were performed in 5% milk in TBST (150 mM NaCl, 20 mM Tris-HCl pH 7.6, 0.1% Tween-20). Primary antibodies used in this study are: anti-Rab5a (Santa Cruz, SC-46692), anti-Rab11b (Thermo Fisher Scientific, PA531348), anti-Atp6v0l (Bio-technie, NBP1-89342), anti-Atp6v1a (Thermo Fisher Scientific, MA527730), anti-Synapsin1 (Synaptic Systems, 106002), anti-PSD95 (Synaptic Systems, 124011), anti-VGLUT1 (Synaptic Systems, 135302), anti-VGAT1 (Synaptic Systems, 131003), and anti-VAMP2 (Synaptic Systems, 104211). Chemiluminescent detection was carried out using a Chemidoc MP imaging system (Bio-Rad) with Western Sun (Cyanagen XLS063,0250) or Western Antares (Cyanagen XLS141,0250) substrates.

#### ***Sample preparation for proteomic analysis***

Proteins were digested following the FASP (Filter Aided Sample Preparation) protocol [35]: disulfide bonds of cysteines were reduced with an incubation at 95 °C for 1 min with 50 µl of 0.1 M DTE (1,4-dithioerythritol) in Tris/HCl pH 7.4. After two centrifugation steps on Amicon Ultra-3K at 14,000 × g for 10 min with a solution of urea 8 M, cysteine residues were alkylated with 100 µl 0.05 M IAA (iodoacetamide) in urea 8 M. Samples were centrifuged twice on Amicon Ultra-3K at 14,000 × g for 10 min with a solution of urea 8 M and then incubated overnight at 37 °C in the presence of sequencing grade trypsin (Sigma-Aldrich, St Louis, MO) 1:50 (w/w), upon dilution of urea up to 2 M with 50 mM ammonium bicarbonate buffer. The obtained peptides were subsequently desalted using home-made Stage Tips C18.

#### ***LC-MS/MS Analysis***

Desalted peptides were injected in a capillary chromatographic system (Vanquish™ Neo UHPLC System, Thermo Fisher Scientific) for peptide separations on a 75 µm i.d. × 15 cm reverse phase silica capillary column, packed with 1.9 µm ReproSil-Pur 120 C18-AQ (Dr. Maisch GmbH, Germany). A 100 min-gradient of eluents A (pure water with 0.1% v/v formic acid) and B (acetonitrile with 0.1% v/v formic acid) was used to achieve separation (from 3% to 29% of B in 88 min, 300 nL/min flow rate). MS analyses were performed using a Q-Exactive mass spectrometer (Thermo Scientific, Bremen, Germany) equipped with a nano-electrospray ion source (Proxeon Biosystems). Each sample was analysed in technical triplicates for label-free quantitative proteomics. Full scan spectra were

acquired with the lock-mass option, resolution set to 70,000 and mass range from  $m/z$  300 to 2000. The ten most intense ions (charge exclusion: unassigned, 1, 6-8, >8) were selected to be fragmented (ddMS2). MS/MS spectra were acquired with resolution set to 17,500, NCE set to 25 with an isolation window of 2  $m/z$ .

#### ***Data Processing and statistical analysis***

Raw data were then analysed by MaxQuant software (v. 1.6.1.0) [36] for label-free protein quantification based on the precursor intensity. Searches were performed with the following settings: trypsin as proteolytic enzyme; 2 missed cleavages allowed; carbamidomethylation on cysteine as fixed modification; protein N-terminus-acetylation and methionine oxidation as variable modifications; mass tolerance was set to 5 ppm and to 20 ppm for precursor and fragment ions, respectively; mouse\_proteome\_20220525 (63,641 sequences; 28,558,480 residues) was used as database. FDR (False Discovery Rate) of 1% was selected for both peptide and protein identification, with minimum two peptides per protein with at least one unique. The complete dataset of identified and quantified proteins was processed using an in-house developed R script as follows: log transformation; filtering for proteins with at least 50% quantification rate in one or more conditions; imputation of missing values. ANOVA post-hoc with Tukey correction was performed to detect the dysregulated proteins. GO (Gene Ontology) analyses were performed using David software, freely available [37] setting a list of proteins known to be expressed in brain.

### **3. Results**

#### ***3.1. Identification of Distinct Differential Expression Patterns and Functional Gene Clusters in the Developing Cortex***

To define the transcriptomic profile of genes deregulated during early phases of cortical development, we extracted total RNA from females and male's littermates at E16 (embryonic day 16), P5 (postnatal day 5) and P10 (postnatal day 10) corresponding to the peak of neurogenesis, neuronal differentiation and early synaptogenesis, and synaptic maturation with circuit refinement, respectively. RNA samples were then subjected to sequencing using Illumina NextSeq6000 system and analyzed to identify differentially expressed genes. Principal Component Analysis (PCA) revealed a clear separation among the three different time points (Supplementary Figure 1A), indicating significant changes in the transcriptomic landscape throughout brain development. A total of 8766 genes were found differentially expressed (DEGs) along our time windows with a  $p$ -adjusted < 0.05. In detail, when comparing the transcriptomic profiles to the early E16 stage, P5 exhibited 7690 deregulated genes, with 3829 showing increased expression (up-regulated) and 3861 showing decreased expression (down-regulated) (Supplementary Figure 1B). As development progressed to P10, we observed a total of 8182 DEGs (4081 up-regulated and 4101 down-regulated genes) (Supplementary Figure 1C). Remarkably, a direct comparison between P10 and P5 revealed a less extensive genetic remodeling, with 5855 genes undergoing deregulation (3040 up-regulated and 2815 down-regulated genes at P10) (Supplementary Figure 1D), suggesting a major shift in the transcripts composition of cortical tissue occurring between P5 and E16. A comprehensive examination of transcriptional profiles evidenced six distinct patterns throughout the cortical development (Figure 1A). In detail, genes enriched in clusters 1, 2 and 3 are predominantly downregulated at E16, but their expression rises at P5 and P10 (Figure 1A). Gene ontology (GO) analysis of these genes revealed enrichment for pathways related to mitochondrial and synaptic function as well as neurotransmitter processing (Figure 1B). In contrast, transcripts in clusters 4, 5 and 6 are highly expressed at E16 but decrease in P5 and/or P10 (Figure 1A), with GO terms highlighting processes such as response to nerve growth factor, mRNA processing and metabolism. Notably, some pathways including axonogenesis and neuron projection resulted enriched across clusters 1, 3 and 5, indicating that they do not share a uniform expression profile throughout cortical development (Figure 1A,B). Interestingly, autophagy-related processes were significantly dysregulated during cortical maturation (Figure 1B and Supplementary Figure 2). Specifically, autophagy transcripts were

enriched in clusters 2, 3, and 4, reflecting differential regulation at early developmental stages and a common upregulation at P10 (Figure 1A,B).

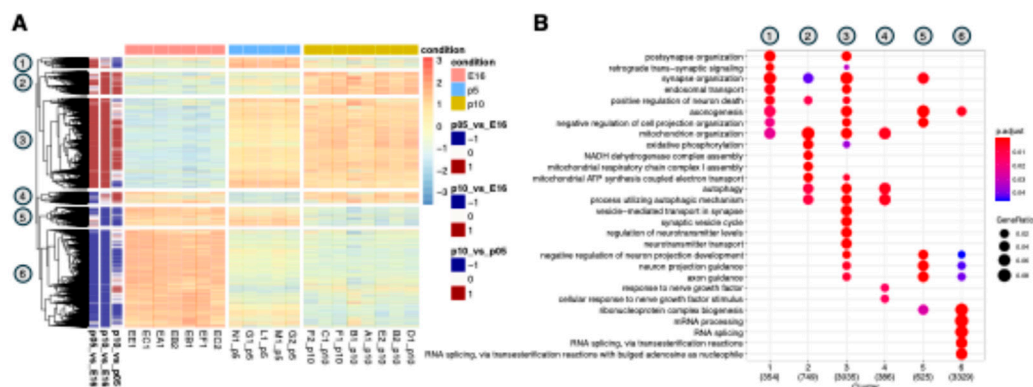


**Figure 1. Coordinated pathway networks drive cortical development. (A)** Heatmap showing the relative transcript levels of all differentially expressed genes (DEGs, rows) across developmental stages (columns). Columns are grouped into three major developmental time points: E16, P5, and P10. Red indicates high gene expression, and blue indicates low expression. **(B)** Dot plot depicting the biological processes enriched within the six clusters identified by hierarchical clustering of the expression data (\*p adj < 0.05).

Further investigation of the transcriptomic dataset identified 274 DEGs associated to autophagy (GO:0006914). Clustering of these genes reveals five distinct temporal profiles during cortical development, thus confirming that autophagy is regulated through subsets of genes active at specific developmental windows (Figure 2A). For instance, clusters 1 and 2 showed a trend of low expression at E16, which increases progressively at P5 and P10, indicating that these autophagy-related genes become more active during postnatal brain development, probably contributing to processes such as circuit maturation, neuronal connectivity and synaptic plasticity. In contrast, cluster 3 displayed a different pattern, with high expression at E16, a peak at P5 and a decline by P10. This trajectory implies a different functional role for these genes, likely becoming more critical during the transition from embryonic to early postnatal stages of brain maturation. Cluster 4 was characterized by genes that were highly expressed at E16, followed by gradual decrease at P5 and P10, indicating a stronger involvement during early embryonic development. Finally, Cluster 5 exhibited similar trends, with high levels at E16, a decrease at P5 and a modest increase at P10. This pattern suggests that these autophagy processes are highly active during embryonic development, temporarily downregulated during early postnatal stages, and re-engaged during later phases of neuronal maturation, possibly in relation to synaptic remodeling, circuit refinement, or neuronal homeostasis. Overall, these expression dynamics point to a developmental shift in the transcriptomic profile of autophagy-related genes, from certain genes being predominantly active during embryogenesis, to a different subset gaining relevance in the postnatal brain. This underscores the dynamic and complex regulation of autophagy throughout brain development. To gain into the biological processes of these clustered genes, we performed GO analysis of DEGs within each group. The results revealed that mTOR signaling pathway is highly represented in cluster 1 and 4, while LKB1 and AMPK are more significantly enriched in cluster 4. NGF-signaling via TRKA and Interleukin-5 signaling were also enriched in cluster 1. Processes related to autophagy regulation and cellular senescence were prominently represented in cluster 1, 2 and 4. Cluster 3 was specifically enriched in DEGs involved in TP53 network. Phosphatidylinositol metabolism and biosynthesis were mainly confined to cluster 5, along with pathways associated with angiogenesis.

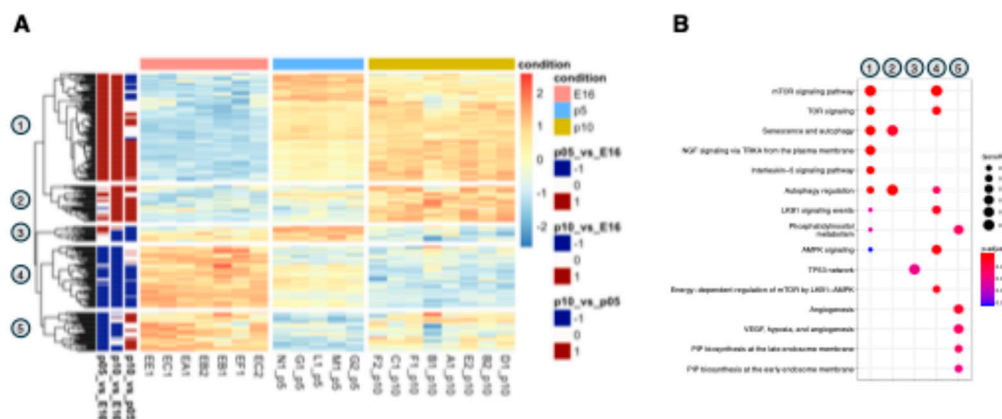


**Figure 2. Autophagy is dynamically regulated during cortical development. (A)** Heatmap showing the scaled expression of 274 autophagy genes divided into five clusters. It visually represents gene expression levels across different developmental stages: E16 (embryonic day 16.5), P5 (postnatal day 5), and P10 (postnatal day 10). **(B)** Dot plot of Gene Ontology (GO) enriched pathway analysis in developing cortices, indicating the top 30 most enriched pathways. The graph highlights that different biological processes drive the signature of each cluster (\* $p$  adj < 0,05).

To better delineate the autophagy gene network dynamics during brain development, we performed a Gene Set Enrichment Analysis (GSEA) on a curated autophagy gene list as defined in the work of Bordi and colleagues [18]. In brief, they categorized 604 genes into seven main functional groups: (i) mTOR and upstream signaling pathways, (ii) core autophagy machinery, (iii) autophagy regulators, (iv) mitophagy-related genes, (v) docking and fusion components, (vi) lysosomal genes, and (vii) lysosomal-related genes. As depicted by the dot plot in Supplementary Figure 3A, the comparison P10 vs E16 showed the most significant enrichment in gene sets related to lysosome and lysosome-related genes (indicated by large, dark red dots with asterisks), thus suggesting a substantial upregulation of these pathways between the embryonic stage (E16) and postnatal day 10 (P10). The comparison P10 vs P5 displayed significant enrichment also for autophagy regulators indicating that the autophagy machinery is more tightly controlled as the brain matures. In contrast, the P5 vs E16 comparison manifested a much lower degree of enrichment. Overall, these data confirmed a temporal shift in the regulation of autophagy and lysosomal pathways during cortical development, becoming more active and well-regulated as the brain transits from early embryonic stages to postnatal life, with the most significant changes occurring between P5 and P10. To confirm these findings, we measured the mRNA levels in cortices at E16, P5 and P10 collected from males and females separately (Figure 3). Real-time qPCR of autophagy regulator genes showed that the expression of *c-Fos*, *Bdnf* and *Egr1* highly increases from E16 to P10. Similarly, *Pgc1a* and *Tfeb* displayed a notable upregulation at P10 compared to the earlier stages. In contrast, *Foxo1*, *Foxo3*, *Hif1a* and *Tfe3* exhibited little to no change across all time points (Figure 3A,B).

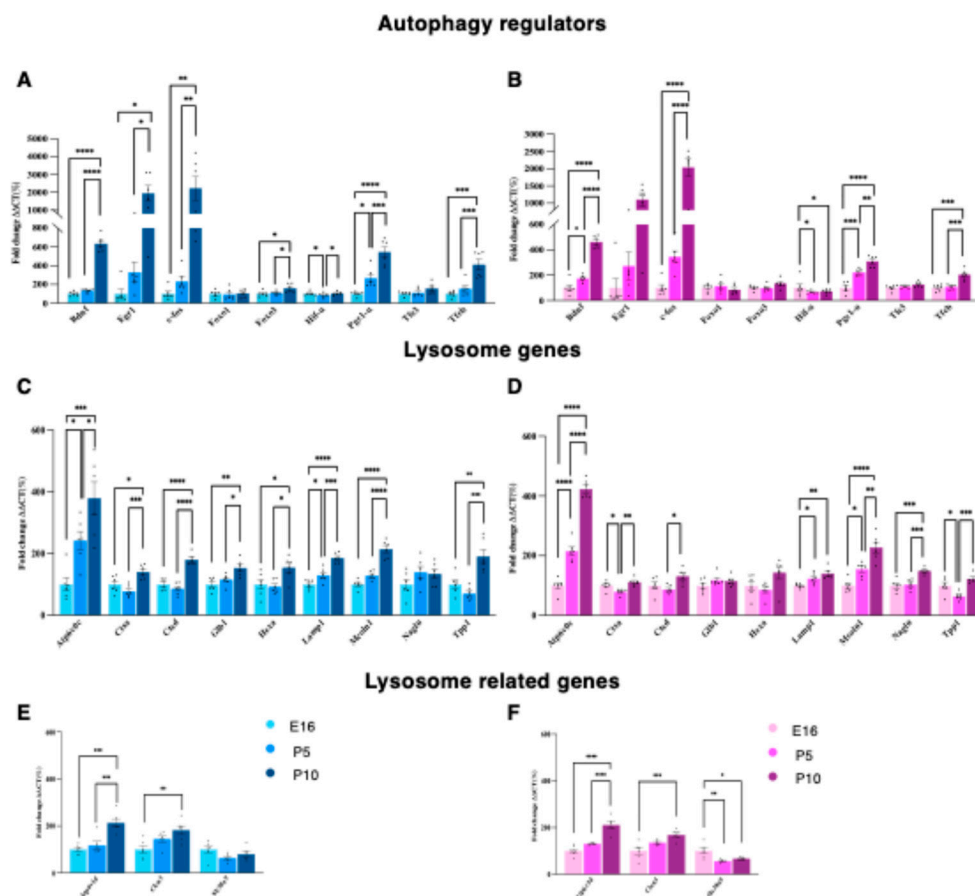


**Figure 3. Lysosomal and autophagy gene expression during cortical development is sex independent.** Transcriptomic profiles of the autophagy and lysosomal genes in developing male and female cortices. **(A and B)** Bar graph showing the mRNA levels of autophagy regulator genes in male at embryonic (E16, light blue), early postnatal (P5, medium blue), and later postnatal (P10, dark blue) stages **(A)** and female (E16, pink), early postnatal (P5, dark pink), and later postnatal (P10, violet) **(B)**. **(C and D)** Developmental mRNA expression of lysosomal genes. Bar graphs illustrate the relative expression of representative lysosomal and lysosomal related genes in males **(C and E)** and females **(D and F)** across the same time points. Gene expression was normalized to the housekeeping gene cyclophilin and is presented as fold change relative to E16 levels (set as 100%). Data are shown as mean  $\pm$  SEM from  $n = 6$  biological replicates. Statistical significance was assessed using one-way ANOVA followed by Tukey's post hoc test,  $p < 0.05$  was considered significant.

Lysosomal and related genes manifest an overall higher expression at P10 compared to E16 and P5 as illustrated in Figure 4C–F. Although the group of “core autophagic genes” was not statistically significant in the GSEA analysis (Supplementary Figure 3A), we decided to test the mRNA levels of some key components. Indeed, the mRNA levels of *Atg9a* and *Sqstm1* increased at P10 compared to P5 and E16 (Supplementary Figure 3B,C). The expression of *Atg16l*, *Gabarapl1*, and *Lc3* decreases between E16 and P5, with either no change or a slight increase observed at P10 (Supplementary Figure 3B,C). Conversely, the *Ulk1* shows the opposite pattern, significantly decreasing from the embryonic to the postnatal stage (Supplementary Figure 3B,C). Collectively, these results indicate a developmental shift in gene expression, where the increase in autophagy and lysosomal function genes observed in both male and female mice from E16 to P10 likely reflects the heightened metabolic and cellular housekeeping demands of the maturing brain that coincides with synaptogenesis window.

### 3.2. Mapping the Correlation Between Autophagy and Synaptic Architecture in the Postnatal Cortex.

To investigate the functional relationship between autophagy and synaptic function, we conducted a gene co-expression analysis. Specifically, we selected biological processes significantly associated with either autophagy or synaptic activity and calculated the mean pairwise correlation among genes annotated to these processes. As indicated by the heatmap, a strong correlation emerged between these two pathways (pearson's correlation coefficients between 0.90 and 0.99, correlation tests p-values between  $4.4e-09$  and  $5.6e-25$ ) (Supplementary Figure 4A,B), thus reinforcing the concept that autophagy is not merely a cellular cleanup mechanism but may also play a crucial role in shaping the complex architecture of synapses. Guided by transcriptomic data, we set out to characterize the dynamics of autophagic proteins associated with the synaptic compartment. To this end, we isolated crude synaptosomes, artificial organelles retaining essential synaptic components, from the cortices of WT mice at three postnatal developmental stages (P5, P10, and P20), which span the onset, progression, and maturation of synaptogenesis, a process that occurs predominantly after birth. We first validated the enrichment of synaptosomal fractions isolated from brain homogenates by analyzing the expression of markers associated with different subcellular compartments (Supplementary Figure 5). Immunoblot analysis revealed a predominant expression of Synapsin 1, as expected, in the P2' fraction. In contrast, the endoplasmic reticulum marker calnexin and the cytosolic protein GAPDH were minimally detected in the same fraction. Notably, the mitochondrial marker TIM23 showed a relatively higher abundance, consistent with previous reports [19,20] (Supplementary Figure 5). To unravel the protein contents that shape these structures during early stages of development, we subjected the cortical purified synaptosomes to advanced mass spectrometry-based proteomics analysis. Three to four independent biological samples per time point were analyzed using a label-free quantitative approach. PCA analysis indicated a clear separation among the three different time points (Supplementary Figure 6A), suggesting that the proteome is extremely different during brain development. A total of 1035 proteins were identified by filtering for those with at least 50% quantification rate in one condition, however the statistically significant differentially expressed proteins (DEPs) were 514. When comparing samples to the early P5 stage, P10 exhibited 126 deregulated proteins (FDR adjusted p-value < 0.05), with 59 showing increased expression (upregulated) and 67 showing decreased expression (downregulated) (Supplementary Figure 6B,C). As development progressed to P20, we observed a substantially greater number of changes relative to P5, with a total of 343 DEPs (293 upregulated and 50 downregulated proteins) (Supplementary Figure 6B,D). Remarkably, a direct comparison between P20 and P10 revealed extensive proteomic remodeling, with 446 proteins undergoing deregulation (398 upregulated and 48 downregulated proteins), suggesting a major shift in the proteomic composition of synaptic structures occurring between P10 and P20 (Supplementary Figure 6B,E; Table 1). Gene ontology analysis consistently identified synaptic compartments as the most prominent across all three comparisons (Supplementary Figure 6F-H). Among these, 46 deregulated proteins were shared (Figure 4A) and were enriched in synaptic-related cellular compartments (Figure 4C) as well as in processes involving glycolysis, calcium transport, and vesicle acidification (Figure 4B-D).

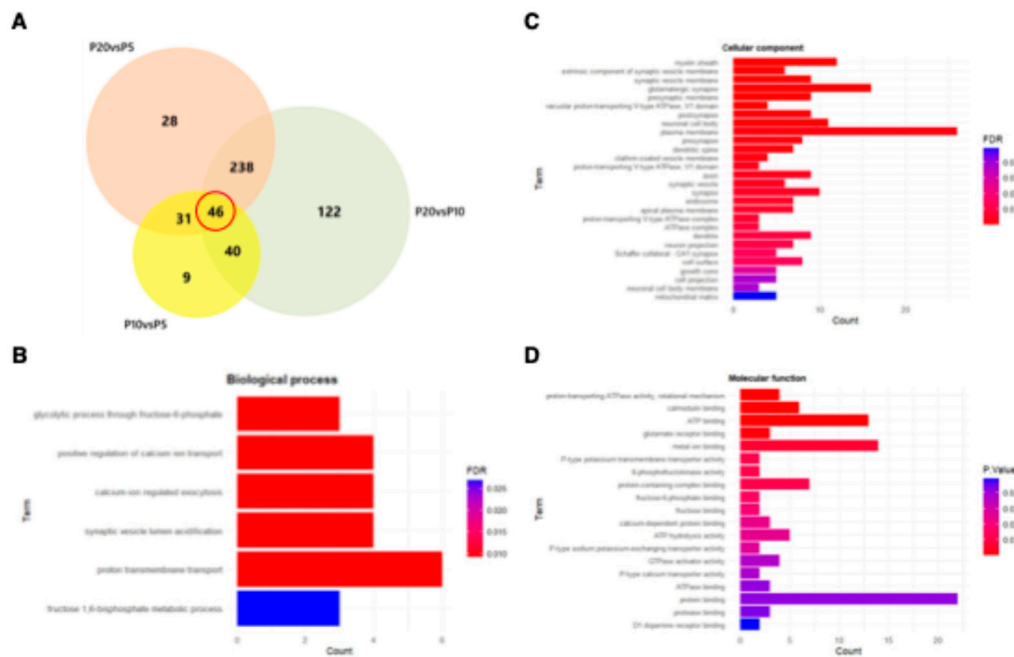


**Figure 4. Comparative analysis of deregulated synaptic proteins across development.** (A) Venn diagram indicating the number of proteins found deregulated among the three comparisons. (B-D) Enriched categories of deregulated proteins are represented by the bar graph for each comparison. The vertical axis shows the top GO terms while the horizontal axis displays the protein counts belonging to each category with  $FDR < 0.05$  (in B and C) and  $p \text{ adj} < 0.05$  (in D).

A deeper investigation of changes in synaptic proteins revealed a total of 181 deregulated proteins in developing cortical synaptosomes (Table 1).

**Table 1.** Summary of significantly deregulated total and synaptic proteins in the developing mouse cortex.

	Significant ( $FDR < 0.05$ )			
	N° of proteins	P10 vs P5	P20 vs P10	P20 vs P5
<b>Total</b>	514	126	446	343
<b>Synaptic</b>	181	31	75	51
<b>%</b>	35	25	17	15

The heatmap of synaptic proteins showed that the majority of these is upregulated at P20 compared to earlier developmental stages (Figure 5A), in line with previous reports [21–23].

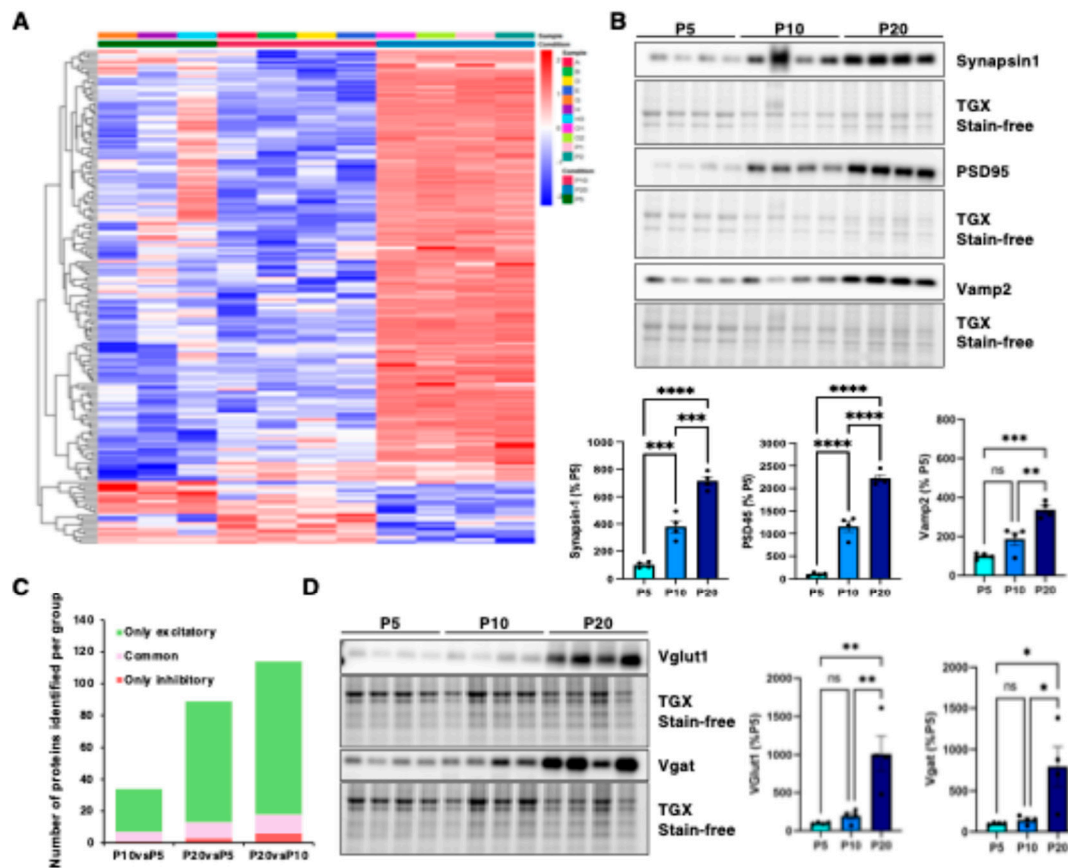


**Figure 5. Synaptic proteins are mostly upregulated in developing wild-type mice cortices.** (A) Heatmap of 181 differentially expressed synaptic proteins. Red color indicates high expression; blue indicates low expression. (B) Protein expression levels of Synapsin1, VAMP2 (pre-synaptic markers) and PSD95 (post-synaptic compartment marker) were measured by western blot at three stages of cortical development: P5, P10, and P20. (C) Bar graph showing the number of excitatory, inhibitory, and shared synaptic proteins in each comparison. (D) Immunoblotting showing the expression levels of V-GLUT1 (marker of glutamatergic synapses) and V-GAT (marker for inhibitory synapses) during cortical development (P5, P10 and P20). The protein levels were normalized to the total protein lysates. Data are shown as the mean  $\pm$  SEM (n=4). One way ANOVA followed by Tukey's test. \* $p < 0,05$ , \*\* $p < 0,01$  and \*\*\* $p < 0.0001$ .

Moreover, hierarchical clustering identified two distinct groups: cluster 1 comprises proteins selectively upregulated at P20, whereas cluster 2 includes proteins that are predominantly downregulated at later stages of development. (Figure 5A). To confirm these dynamics, we measured the expression levels of key synaptic proteins across the selected time periods. As shown by the western blot, pre-synaptic Synapsin 1 exhibited a progressive and statistically significant increase in expression levels. Specifically, an upregulation was observed from P5 to P10 (\*\* $p < 0.001$ ) followed by a further elevation from P10 to P20 (\*\* $p < 0.01$ ) (Figure 5B). This pattern is consistent with the expansion in synaptic density and the increasing complexity of presynaptic terminals during cortical maturation. Similarly, the Vesicle-associated membrane protein 2 (VAMP2) increased its expression during the developmental stages (Figure 5B). Finally, the post-synaptic marker, PSD95 (Postsynaptic density protein 95) displayed a significant upregulation between P5 and P10 (\*\*\*\* $p < 0.0001$ ) and between P10 and P20 (\*\*\*\* $p < 0.0001$ ) (Figure 5B), reflecting the maturation and organization of the postsynaptic density in conjunction with the formation and strengthening of synapses. Notably, a subset (n = 159) of the deregulated proteins was annotated in SynGO and subdivided into six categories (Supplementary Figure 7A). The majority of these proteins is presynaptic or involved in synaptic organization (Supplementary Figure 7B). We further characterized the synaptosomes nature along cortical development by determining the changes in excitatory and inhibitory synaptic

markers. Among the significantly altered proteins, a total of 106 were ascribed to glutamatergic synapses exclusively, while 7 were uniquely defined as GABA-ergic; 14 proteins could function as both excitatory and inhibitory synapse (Figure 5C). As evidenced in Figure 5D, the expression of V-GLUT1 (Vesicular Glutamate Transporter), a key indicator of glutamatergic synapses, was augmented from P10 to P20 (\*\*p < 0.01). Similarly, V-GAT (Anti-Vesicular GABA Transporter), a marker for inhibitory synapses, showed a significant upregulation from P10 and P20 (Figure 5D). This trend suggested a proliferation and maturation of inhibitory and excitatory synapses during the later stage of brain development. Overall, these data are consistent with the well-known phase of synaptogenesis and synaptic maturation that characterizes the mammalian brain [24–26].

Finally, we examined whether autophagic proteins were enriched in developing cortical synaptosomes. With this aim, we interrogated the dataset using the list reported by Bordi and colleagues (Bordi et al., 2021), as previously done for the transcriptomic analyses. Interestingly, we identified 55 autophagic-lysosomal proteins, 37 of which were significantly deregulated (Table 2).

**Table 2.** Summary of significantly deregulated total and autophagic proteins in the developing mouse cortex.

	Significant (FDR < 0.05 )			
	N° of proteins	P10 vs P5	P20 vs P10	P20 vs P5
<b>Total</b>	514	126	446	343
<b>Autophagy-Lysosomal</b>	37	6	24	15
<b>%</b>	7	5	5	4

They belong to different categories as reported in Figure 6A. Similar to synaptic proteins, their expression increased during brain development (Figure 6B). Notably, several ATP6 synthase subunits showed marked upregulation, suggesting enhanced synaptic acidification, which is consistent with the primary role of synaptic vesicles in neurotransmitter loading and release during neuronal transmission [27]. Western blot analysis confirmed this expression trend for ATP6V1A and ATP6V0A1 in purified synaptosomes across developmental stages (Figure 6C). In addition, diverse Rab proteins were found to be markedly deregulated. Notably, Rab1b, Rab5a, and Rab5c showed increased expression as the cortex matured, whereas Rab11b and Rab14 exhibited the opposite trend (Figure 6B). Changes in protein levels were further validated for Rab5a and Rab11b by immunoblot measurements (Figure 6C). Together, these findings demonstrate a dynamic and developmentally regulated remodeling of the autophagy–lysosomal machinery at cortical synapses. The coordinated upregulation of lysosomal ATP6 synthase subunits and specific Rab GTPases suggests a progressive enhancement of autophagic and endo-lysosomal trafficking capacity during postnatal brain development. This maturation of autophagy-related pathways at synaptic compartments is likely to support synaptic growth, remodeling, and circuit refinement, underscoring a previously underappreciated contribution of autophagy–lysosomal processes to synaptic maturation.

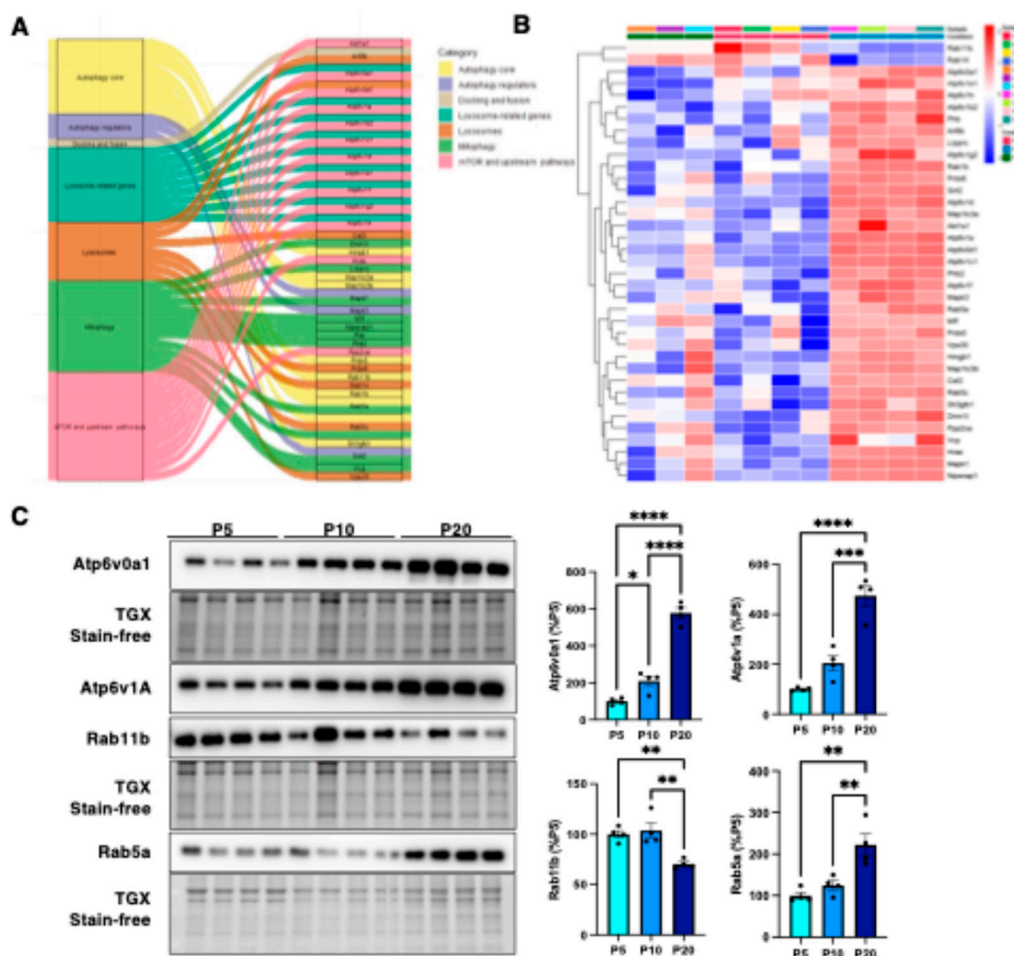


**Figure 6. Autophagy and lysosomal proteins at synaptic site are predominantly upregulated in maturing wild-type cortices.** (A) Alluvial plot showing the different categories of the deregulated autophagy-lysosomal proteins across the developmental maturation, as found in synaptosomes. (B) Heatmap illustrating the expression profile of deregulated autophagy-lysosomal proteins purified from synaptosomes across cortical developmental stages. Red color indicates high expression; blue indicates low expression. (C) Immunoblot from synaptosomal lysates of WT cortices at different stage of post-natal development (P5, P10 and P20). Atp6v0a1, Atp6v1a, Rab5a, and Rab11 signal intensities were quantified by densitometric analysis. Protein levels were normalized to total protein using stain-free technology. Data are shown as the mean  $\pm$  SEM from four biological replicates (n = 4), expressed as a percentage of the P5 mean. Statistical significance was assessed using one-way ANOVA followed by Tukey's post hoc test; \*p < 0.05 was considered significant.

#### 4. Discussion

Over the past decades, the importance of regulatory gene networks in controlling cell metabolism has become evident in every aspect of neuronal functions [28,29]. Despite significant advances in our understanding of the transcriptional regulation of autophagy, the broader gene network orchestrating this pathway in developing neurons remain largely unexplored. Identifying which specific autophagy genes are activated or silenced during distinct stages of brain development could provide valuable insight for designing therapeutic strategies, particularly for neurodevelopmental disorders.

Overall, our transcriptomic analysis indicates that cortical development is driven by an integrated network of pathways, with autophagy emerging as a dynamically regulated component. Accordingly, temporal clustering revealed distinct developmental regulation of autophagy-related genes (GO:0006914) across cortical maturation. Genes in clusters 1 and 2 were progressively upregulated from E16 to P5 and P10, indicating increased postnatal activation of autophagy-related

processes associated with synaptic maturation, neuronal connectivity, and plasticity. These clusters were enriched for mTOR signaling, NGF-TRKA and interleukin-5 signaling, as well as pathways regulating autophagy and cellular senescence, suggesting their predominant deregulation during postnatal development. In contrast, cluster 3 genes peaked during the embryonic-to-early postnatal transition (E16–P5) and were enriched for TP53-associated pathways, indicating a stage-specific role during early brain maturation. Clusters 4 and 5 were characterized by high embryonic expression followed by postnatal downregulation, highlighting pathways predominantly active at early developmental stages. Cluster 4 was enriched for mTOR, LKB1, and AMPK signaling, implicating energy-sensing and autophagy regulation during embryogenesis, whereas cluster 5 was associated with phosphatidylinositol metabolism and angiogenesis, suggesting transient engagement during embryonic development with partial reactivation at later stages.

To narrow our analysis, we followed the expression of a subset autophagy and lysosomal genes during cortical development in both males and females. Notably, we found an overall increase in autophagy-lysosomal genes that was consistent in both male and female mice, underscoring the non-sex-specific effects on development. Moreover, we observed the decreasing expression of Ulk1 from the embryonic stage (E16) to the postnatal stage (P10) in the cortex, thus suggesting a functional shift from processes that heavily rely on high ULK1 activity to those that require its downregulation, particularly during a period of intense neuronal differentiation, synaptogenesis, and circuit maturation.

Growing evidence indicates that autophagy plays an active role in synaptic development and function, extending beyond its canonical role in cellular homeostasis to directly regulate synaptic remodeling and plasticity. Consistent with this notion, our transcriptomic profiling revealed a strong association between autophagy-related genes and synaptic pathways during cortical development. Notably, a targeted interrogation of cortical synaptosomal proteomes using a curated autophagy gene list (Bordi et al., 2021) uncovered a substantial enrichment of autophagy-lysosomal proteins that increased in abundance over developmental time. In particular, the upregulation of multiple ATP6 synthase subunits suggests a progressive enhancement of synaptic acidification, a feature previously linked to synaptic maturation, and circuit refinement. Moreover, the differential regulation of Rab GTPases involved in endo-lysosomal trafficking further supports the idea that precise spatial and temporal control of autophagy-related pathways is required for synaptic development. Together, these findings support recent studies demonstrating that synaptic autophagy contributes to the maturation and remodeling of neuronal circuits and highlight autophagy as a dynamic and integral component of synaptic development in the mammalian cortex.

In conclusion, our findings reveal that autophagy during brain development is tightly integrated with metabolic signaling, synaptic function, and cell fate decisions, underscoring its multifaceted role beyond cellular clearance. The coordinated regulation of autophagy-lysosomal components at synaptic sites point out their contribution to synaptic maturation, remodeling, and circuit refinement. Importantly, synaptic dysfunction is a hallmark of several neurodevelopmental disorders (NDDs), including autism spectrum disorders, epilepsy, and intellectual disabilities, which are frequently associated with impaired synaptic plasticity, altered neurotransmitter receptor composition, and dysregulation of genes governing synapse formation and maintenance. In this context, our data support the notion that aberrant regulation of synaptic autophagy may represent a convergent mechanism underlying neurodevelopmental pathology and suggest that targeting autophagy-related pathways could offer novel therapeutic avenues for disorders characterized by defective synaptic development.

**Supplementary Materials:** The following supporting information can be downloaded at the website of this paper posted on Preprints.org, Figure S1: Transcriptomic profiling of cortical development; Figure S2: Gene Ontology (GO) network showing autophagy and linked pathways. Figure S3: Enrichment analysis of autophagy and lysosomal pathways. Figure S4: Autophagy and synaptic related processes are co-regulated during cortical

maturation. Figure S5: Synaptosomal enrichment analysis. Figure S6: Proteomic profiling of developing cortical synaptosomes. Figure S7: Functional and spatial distribution of synaptic proteins.

**Author Contributions:** **Francesca Nuzzolillo:** formal analysis, methodology, validation, writing – original draft, writing – review & editing; **Clarissa Braccia:** formal analysis, methodology, validation, writing – original draft, writing – review & editing; **Stefano de Pretis:** formal analysis, data curation, writing – review & editing; **Annapaola Andolfo:** formal analysis, data curation, writing – review & editing; **Michela Palmieri:** conceptualization, investigation, funding acquisition, methodology, project administration, supervision, visualization, writing – original draft, writing – review & editing. The authors have reviewed and edited the output and take full responsibility for the content of this publication.

**Funding:** This work was supported by the Ministry of University and Research, grant n. MSCA\_0000082 to MP.

**Institutional Review Board Statement:** The study was conducted in accordance with the Declaration of Helsinki. The animal study protocol was approved by the Institutional Minister of Health (IACUC #002/18).

**Data Availability Statement:** The datasets produced in this study are available in the following databases: RNA-Seq data: Gene Expression Omnibus # Proteomic data.

**Acknowledgments:** We would like to acknowledge the Charles River animal facility at the San Raffaele Research Institute (IRCCS Ospedale San Raffaele) for their technical support and assistance with animal care and maintenance.

**Conflicts of Interest:** The authors declare no conflicts of interest.

## Abbreviations

The following abbreviations are used in this manuscript:

mTOR	(mechanistic target of rapamycin)
AMPK	(AMP-activated protein kinase)
ULK1	(Unc-51 Like Autophagy Activating Kinase 1)
LKB1	(Liver Kinase B1)
SEM	(Standard Error of the Mean)
NGF	(Nerve Growth Factor)
TRKA	(Tyrosine kinase A)

## References

1. Dikic, I.; Elazar, Z. Mechanism and medical implications of mammalian autophagy. *Nat. Rev. Mol. Cell Biol.* **2018**, *19*, 349–364. <https://doi.org/10.1038/s41580-018-0003-4>.
2. Stavoe, A.K.H.; Holzbaur, E.L.F. Autophagy in Neurons. *Annu. Rev. Cell Dev. Biol.* **2019**, *35*, 477–500. <https://doi.org/10.1146/annurev-cellbio-100818-125242>.
3. Palmer, J.E.; Wilson, N.; Son, S.M.; Obrocki, P.; Wrobel, L.; Rob, M.; Takla, M.; Korolchuk, V.I.; Rubinsztein, D.C. Autophagy, aging, and age-related neurodegeneration. *Neuron* **2025**, *113*, 29–48. <https://doi.org/10.1016/j.neuron.2024.09.015>.
4. Ventruti, A.; Cuervo, A.M. Autophagy and neurodegeneration. *Curr. Neurol. Neurosci. Rep.* **2007**, *7*, 443–451.
5. Son, J.H.; Shim, J.H.; Kim, K.H.; Ha, J.Y.; Han, J.Y. Neuronal autophagy and neurodegenerative diseases. *Exp. Mol. Med.* **2012**, *44*, 89–98. <https://doi.org/10.3858/emm.2012.44.2.031>.

6. Xi, Y.; Dhaliwal, J.S.; Ceizar, M.; Vaculik, M.; Kumar, K.L.; Lagace, D.C. Knockout of Atg5 delays the maturation and reduces the survival of adult-generated neurons in the hippocampus. *Cell Death Dis.* **2016**, *7*, e2127. <https://doi.org/10.1038/cddis.2015.406>.
7. Coupé, B.; Ishii, Y.; Dietrich, M.O.; Komatsu, M.; Horvath, T.L.; Bouret, S.G. Loss of autophagy in pro-opiomelanocortin neurons perturbs axon growth and causes metabolic dysregulation. *Cell Metab.* **2012**, *15*, 247–255. <https://doi.org/10.1016/j.cmet.2011.12.016>.
8. Nikolettou, V.; Sidiropoulou, K.; Kallergi, E.; Dalezios, Y.; Tavernarakis, N. Modulation of autophagy by BDNF underlies synaptic plasticity. *Cell Metab.* **2017**, *26*, 230–242.e5. <https://doi.org/10.1016/j.cmet.2017.06.005>.
9. Torres, C.A.; Sulzer, D. Macroautophagy can press a brake on presynaptic neurotransmission. *Autophagy* **2012**, *8*, 1540–1541. <https://doi.org/10.4161/auto.21330>.
10. Tang, G.; Gudsnuk, K.; Kuo, S.-H.; Cotrina, M.L.; Rosoklija, G.; Sosunov, A.; Sonders, M.S.; Kanter, E.; Castagna, C.; Yamamoto, A.; Yue, Z.; Arancio, O.; Peterson, B.S.; Champagne, F.; Dwork, A.J.; Goldman, J.; Sulzer, D. Loss of mTOR-dependent macroautophagy causes autistic-like synaptic pruning deficits. *Neuron* **2014**, *83*, 1131–1143. <https://doi.org/10.1016/j.neuron.2014.07.040>.
11. Ebrahimi-Fakhari, D.; Saffari, A.; Wahlster, L.; Lu, J.; Byrne, S.; Hoffmann, G.F.; Jungbluth, H.; Sahin, M. Congenital disorders of autophagy: an emerging novel class of inborn errors of neuro-metabolism. *Brain* **2016**, *139*, 317–337. <https://doi.org/10.1093/brain/awv371>.
12. Fassio, A.; Falace, A.; Esposito, A.; Aprile, D.; Guerrini, R.; Benfenati, F. Emerging role of the autophagy/lysosomal degradative pathway in neurodevelopmental disorders with epilepsy. *Front. Cell. Neurosci.* **2020**, *14*, 39. <https://doi.org/10.3389/fncel.2020.00039>.
13. Esposito, A.; Seri, T.; Breccia, M.; Indrigo, M.; De Rocco, G.; Nuzzolillo, F.; Denti, V.; Pappacena, F.; Tartaglione, G.; Serrao, S.; Paglia, G.; Murru, L.; de Pretis, S.; Cioni, J.-M.; Landsberger, N.; Guarnieri, F.C.; Palmieri, M. Unraveling autophagic imbalances and therapeutic insights in Mecp2-deficient models. *EMBO Mol. Med.* **2024**, *16*, 2795–2826. <https://doi.org/10.1038/s44321-024-00151-w>.
14. Zhu, Y.; Runwal, G.; Obrocki, P.; Rubinsztein, D.C. Autophagy in childhood neurological disorders. *Dev. Med. Child Neurol.* **2019**, *61*, 639–645. <https://doi.org/10.1111/dmcn.14092>.
15. Palmieri, M.; Impey, S.; Kang, H.; di Ronza, A.; Pelz, C.; Sardiello, M.; Ballabio, A. Characterization of the CLEAR network reveals an integrated control of cellular clearance pathways. *Hum. Mol. Genet.* **2011**, *20*, 3852–3866. <https://doi.org/10.1093/hmg/ddr306>.
16. Sardiello, M.; Palmieri, M.; di Ronza, A.; Medina, D.L.; Valenza, M.; Gennarino, V.A.; Di Malta, C.; Donaudo, F.; Embrione, V.; Polishchuk, R.S.; Banfi, S.; Parenti, G.; Cattaneo, E.; Ballabio, A. A gene network regulating lysosomal biogenesis and function. *Science* **2009**, *325*, 473–477. <https://doi.org/10.1126/science.1174447>.
17. Raben, N.; Puertollano, R. TFEB and TFE3: linking lysosomes to cellular adaptation to stress. *Annu. Rev. Cell Dev. Biol.* **2016**, *32*, 255–278. <https://doi.org/10.1146/annurev-cellbio-111315-125407>.
18. Bordi, M.; De Cegli, R.; Testa, B.; Nixon, R.A.; Ballabio, A.; Cecconi, F. A gene toolbox for monitoring autophagy transcription. *Cell Death Dis.* **2021**, *12*, 1044. <https://doi.org/10.1038/s41419-021-04121-9>.
19. Picone, P.; Porcelli, G.; Bavisotto, C.C.; Nuzzo, D.; Galizzi, G.; Biagio, P.L.S.; Bulone, D.; Di Carlo, M. Synaptosomes: new vesicles for neuronal mitochondrial transplantation. *J. Nanobiotechnology* **2021**, *19*, 6. <https://doi.org/10.1186/s12951-020-00748-6>.
20. Plum, S.; Eggers, B.; Helling, S.; Stepath, M.; Theiss, C.; Leite, R.E.P.; Molina, M.; Grinberg, L.T.; Riederer, P.; Gerlach, M.; May, C.; Marcus, K. Proteomic Characterization of Synaptosomes from Human Substantia Nigra Indicates Altered Mitochondrial Translation in Parkinson's Disease. *Cells* **2020**, *9*. <https://doi.org/10.3390/cells9122580>.
21. Gonzalez-Lozano, M.A.; Klemmer, P.; Gebuis, T.; Hassan, C.; van Nierop, P.; van Kesteren, R.E.; Smit, A.B.; Li, K.W. Dynamics of the mouse brain cortical synaptic proteome during postnatal brain development. *Sci. Rep.* **2016**, *6*, 35456. <https://doi.org/10.1038/srep35456>.
22. van Oostrum, M.; Blok, T.M.; Giandomenico, S.L.; Tom Dieck, S.; Tushev, G.; Fürst, N.; Langer, J.D.; Schuman, E.M. The proteomic landscape of synaptic diversity across brain regions and cell types. *Cell* **2023**, *186*, 5411–5427.e23. <https://doi.org/10.1016/j.cell.2023.09.028>.

23. Dahlhaus, M.; Li, K.W.; van der Schors, R.C.; Saiepour, M.H.; van Nierop, P.; Heimel, J.A.; Hermans, J.M.; Loos, M.; Smit, A.B.; Levelt, C.N. The synaptic proteome during development and plasticity of the mouse visual cortex. *Mol. Cell. Proteomics* **2011**, *10*, M110.005413. <https://doi.org/10.1074/mcp.M110.005413>.
24. Tau, G.Z.; Peterson, B.S. Normal development of brain circuits. *Neuropsychopharmacology* **2010**, *35*, 147–168. <https://doi.org/10.1038/npp.2009.115>.
25. Zhang, Z.; Jiao, Y.Y.; Sun, Q.Q. Developmental maturation of excitation and inhibition balance in principal neurons across four layers of somatosensory cortex. *Neuroscience* **2011**, *174*, 10–25. <https://doi.org/10.1016/j.neuroscience.2010.11.045>.
26. Chen, J.L.; Villa, K.L.; Cha, J.W.; So, P.T.C.; Kubota, Y.; Nedivi, E. Clustered dynamics of inhibitory synapses and dendritic spines in the adult neocortex. *Neuron* **2012**, *74*, 361–373. <https://doi.org/10.1016/j.neuron.2012.02.030>.
27. Gowrisankaran, S.; Milosevic, I. Regulation of synaptic vesicle acidification at the neuronal synapse. *IUBMB Life* **2020**, *72*, 568–576. <https://doi.org/10.1002/iub.2235>.
28. Maestro, I.; Boya, P.; Martinez, A. Serum- and glucocorticoid-induced kinase 1, a new therapeutic target for autophagy modulation in chronic diseases. *Expert Opin. Ther. Targets* **2020**, *24*, 231–243. <https://doi.org/10.1080/14728222.2020.1730328>.
29. Galluzzi, L.; Pietrocola, F.; Levine, B.; Kroemer, G. Metabolic control of autophagy. *Cell* **2014**, *159*, 1263–1276. <https://doi.org/10.1016/j.cell.2014.11.006>.
30. Bolger, A.M.; Lohse, M.; Usadel, B. Trimmomatic: A flexible trimmer for Illumina sequence data. *Bioinformatics* **2014**, *30*, 2114–2120. <https://doi.org/10.1093/bioinformatics/btu170>.
31. Dobin, A.; Davis, C.A.; Schlesinger, F.; Drenkow, J.; Zaleski, C.; Jha, S.; Batut, P.; Chaisson, M.; Gingeras, T.R. STAR: ultrafast universal RNA-seq aligner. *Bioinformatics* **2013**, *29*, 15–21. <https://doi.org/10.1093/bioinformatics/bts635>.
32. Liao, Y.; Smyth, G.K.; Shi, W. featureCounts: an efficient general purpose program for assigning sequence reads to genomic features. *Bioinformatics* **2014**, *30*, 923–930. <https://doi.org/10.1093/bioinformatics/btt656>.
33. Love, M.I.; Huber, W.; Anders, S. Moderated estimation of fold change and dispersion for RNA-seq data with DESeq2. *Genome Biol.* **2014**, *15*, 550. <https://doi.org/10.1186/s13059-014-0550-8>.
34. Xu, S.; Hu, E.; Cai, Y.; Xie, Z.; Luo, X.; Zhan, L.; Tang, W.; Wang, Q.; Liu, B.; Wang, R.; Xie, W.; Wu, T.; Xie, L.; Yu, G. Using clusterProfiler to characterize multiomics data. *Nat. Protoc.* **2024**, *19*, 3292–3320. <https://doi.org/10.1038/s41596-024-01020-z>.
35. Wiśniewski, J.R.; Zougman, A.; Nagaraj, N.; Mann, M. Universal sample preparation method for proteome analysis. *Nat. Methods* **2009**, *6*, 359–362. <https://doi.org/10.1038/nmeth.1322>.
36. Cox, J.; Neuhauser, N.; Michalski, A.; Scheltema, R.A.; Olsen, J.V.; Mann, M. Andromeda: a peptide search engine integrated into the MaxQuant environment. *J. Proteome Res.* **2011**, *10*, 1794–1805. <https://doi.org/10.1021/pr101065j>.
37. Sherman, B.T.; Hao, M.; Qiu, J.; Jiao, X.; Baseler, M.W.; Lane, H.C.; Imamichi, T.; Chang, W. DAVID: a web server for functional enrichment analysis and functional annotation of gene lists (2021 update). *Nucleic Acids Res.* **2022**, *50*, W216–W221. <https://doi.org/10.1093/nar/gkac194>.

**Disclaimer/Publisher's Note:** The statements, opinions and data contained in all publications are solely those of the individual author(s) and contributor(s) and not of MDPI and/or the editor(s). MDPI and/or the editor(s) disclaim responsibility for any injury to people or property resulting from any ideas, methods, instructions or products referred to in the content.